INTERNATIONAL ATOMIC ENERGY AGENCY
UNITED NATIONS EDUCATIONAL, SCIENTIFIC AND CULTURAL ORGANIZATION
INTERNATIONAL CENTRE FOR THEORETICAL PHYSICS
I.C.T.P., P.O. BOX 586, 34100 TRIESTE, ITALY, CABLE CENTRATOM TRIESTE

SMR/402 - 30

COLLEGE ON SOIL PHYSICS
9 - 27 October 1989

"Numerical Modeling of Coupled Heat and Water Flows during Drying in a Stratified Bare Soil-Comparison with Field Observations"

M. VAUCLIN
Institut de Mécanique de Grenoble
C.N.R.S.
Saint Martin d'Hères
France

Please note: These are preliminary notes intended for internal distribution only.

Journal of Hydrology, 105 (1989) 109–138
Elsevier Science Publishers B.V., Amsterdam — Printed in The Netherlands

NUMERICAL MODELING OF COUPLED HEAT AND WATER FLOWS DURING DRYING IN A STRATIFIED BARE SOIL — COMPARISON WITH FIELD OBSERVATIONS

A. PASSERAT DE SILANS[1]*, L. BRUCKLER[2], J.L. THONY[1] and M. VAUCLIN[1]

[1] *Institut de Mecanique de Grenoble, LA CNRS No.6, B.P. 68, 38402 Saint Martin d'Heres Cedex (France)*

[2] *Institut National de Recherche Agronomique, Station de Sciences du Sol, B.P. 91, Domaine Saint Paul, 84140 Montfavet (France)*

(Received March 7, 1988; accepted for publication April 13, 1988)

ABSTRACT

Passerat de Silans, A., Bruckler, L., Thony, J.L. and Vauclin, M., 1989. Numerical modeling of coupled heat and water flows during drying in a stratified bare soil — Comparison with field observations. J. Hydrol., 105: 109–138.

A general physically based formulation of water — both in liquid and vapor phases — and heat transport in a partially saturated soil coupled with a lower atmosphere boundary layer modeling is presented. It is driven by surface heat and moisture fluxes estimated from meteorological data.

Soil water pressure head and temperature are used as the dependent descriptive variables and the resulting one-dimensional nonlinear equations are solved by a finite element Galerkin method.

The numerical results are compared with field data obtained during an experiment conducted on a 3600 m^2 bare soil presenting three different horizons in the first 80 cm including a crust of 5 mm thick at the soil surface. The plot was intensively equipped with appropriate sensors in order to measure the time evolution of soil temperature, water content and water potential at different depths and locations, the profiles of wind speed, air temperature and vapor pressure above the surface as well as the different radiation components.

Due to experimental uncertainties in the estimation of some parameters (mainly soil hydraulic and thermal properties of the crust) and the lack of determination of others (such as vapor flow coefficients), the model was first calibrated on the first two days of the experimentation and then evaluated on the following five days. For the latter period, very fair agreement between computed and observed values of soil temperature and water content patterns as well as evaporation fluxes demonstrates the reliability of such a model, at least after a calibration phase and, for this specific experimental site, as long as the surface crust is not cracking.

INTRODUCTION

The partially saturated layers of soil near the surface play an important role in many environmental phenomena. They contribute to the partitioning of

* Present address: Centro de Technologia, Universidade Federal de Paraiba, 58000 Joao Pessoa, Paraiba (Brazil)

0022-1694/89/$03.50

NOTATION

a	albedo
C	apparent soil volumetric heat capacity (J m^{-3}K^{-1})
C_{pa}	specific heat of air (J kg^{-1}K^{-1})
D_{va}	molecular diffusivity of water vapor in the air (m^{2}s^{-1})
e	partial vapor pressure (Pa)
$f(\theta)$	pore geometry factor
g	acceleration of gravity (m^{2}s^{-1})
h	water pressure head (m)
j	conversion factor (4.18 J cal^{-1})
K_s	saturated hydraulic conductivity (m s^{-1})
k	von Karman constant (0.4)
L	Monin Obukhov length (m)
M_v	molecular weight of water vapor (kg)
n	porosity
q	soil flux (kg m^{-2}s^{-1}/W m^{-2})
R	perfect gas constant (8.32 J mole^{-1}K^{-1})
R_a	incoming atmospheric radiation (W m^{-2})
Re^*	roughness Reynolds number
R_g	incoming solar radiation (W m^{-2})
r	aerodynamic resistance (s m^{-1})
S	effective saturation of the soil
T	temperature (K)
t	time (s)
u	wind velocity (m s^{-1})
w	gravimetric water content (kg kg^{-1})
W	heat of wetting (J kg^{-1})
z	vertical coordinate (m)
z_0	roughness length (m)
α^*	thermal diffusivity (m^{2}s^{-1})
β	enhancement factor
γ	psychrometric constant (67 Pa K^{-1})
Δh_v	latent heat of vaporization (J kg^{-1})
ε	emissivity
θ	volumetric concentration (m^{3}m^{-3})
λ^*	thermal conductivity (W m^{-1}K^{-1})
μ	mass flow factor/kinematic viscosity (m^{2}s^{-1})
ϕ	specific mass (kg m^{-3})
σ	Stephan Boltzmann constant (5.67 × 10^{-8}W m^{-2}K^{-4})
Γ	tortuosity
Φ	atmospheric flux (kg m^{-2}s^{-1}/W m^{-2})
Ω	stability function

Subscripts

a	air
h	heat
l	liquid
m	momentum
s	surface
v	vapor

precipitation into surface runoff, evaporation and infiltration. They control the conversion of incoming solar and atmospheric radiations into sensible, latent and radiative heat losses. The seed germination and the subsequent root growth strongly depend on both the water content and temperature profiles in the upper soil layers.

Generally speaking, the water and energy balances are linked at the soil atmosphere interface through the evaporation term which in turn is controlled by the climatic conditions and the soil properties as well. Beneath the surface, thermal gradients which may be large close to the surface itself, induce moisture transfers which also affect heat flows. Thus moisture and temperature fields are coupled and a general physically-based model requires that this coupling should be taken into account.

A literature survey shows that several such models generally based on the De Vries (1958) and Luikov (1966) conceptual approaches have been developed in the last fifteen years. Table 1 summarizes some of them, as well as their main characteristics and the applied objectives of their development. The following main features can be observed:

(1) Most of the models are dealing with homogeneous soils, both in the horizontal plane and along the vertical direction, some of them being even not able to consider stratified media, because the water content instead of the water potential is used as the descriptive variable of the mass flow.

(2) The models differ both by the soil physical processes which are taken into account [see soil columns (a), (b), (c) and (d) of Table 1] and by the manner the exchanges between the surface and the atmosphere are considered (see atmosphere and interface columns (a) and (b) respectively in Table 1].

(3) Very few attempts have been made to compare computational results with experimental ones at the proper scale (both in space and time) for which the model is supposed to be used.

The purpose of this paper is to evaluate a relatively general physically based formulation of water and heat transport coupled with a lower atmosphere boundary layer modeling. This evaluation is made by comparing numerical results and field data obtained during a week of drying at several locations on a 3600 m^2 bare soil presenting horizontal stratifications.

THEORY

Soil equations

The approach of Philip and De Vries (1957) modified by Milly (1982) is used as the basis for the formulation of the mathematical model of coupled moisture and heat flows in a partially saturated porous medium. The corresponding equations for one-dimensional vertical movements are summarized in Table 2. See the notation section for symbols used in the paper. This formalism is based on the following assumptions: (H1), the soil is non-swelling, isotropic and chemically inert; (H2), the water is incompressible and chemically pure; (H3),

TABLE 1

Main characteristics of some models available in literature

Authors	Soil system (1)	Soil (2)				Atmosphere (3)		Interface (4)		Validation (5)	Applications (6)
		(a)	(b)	(c)	(d)	(a)	(b)	(a)	(b)		
Sasamori (1970)	B H	CHM	h, T	CD	yes	yes	no	yes	yes	in situ[1]	M
Saugier (1974)	V	CHM	θ, T	CD	no	yes	no	yes	yes	in situ[2]	PP
Rosema (1975)	B H	CHM	h, T	CD	yes	yes	no	yes	yes	none	RS
Van Bavel and Hillel (1976)	B H	UCHM	h, T	CD	no	yes	no	yes	yes	none	SP
Soer (1977)	V H	UCHM	h, T	CD	no	yes	no	yes	yes	in situ[3]	RS
Vauclin et al. (1977)	B H	CHM	h, T	CD	no	yes	no	yes	yes	none	SP
Sophocleous (1979)	B H	CHM	h, T	CD CV DIS	yes	no	no	mass flux and T_s prescribed		in situ[4]	SP
Milly (1982)	B H	CHM	h, T	CD CV DIS	yes	no	no	fluxes prescribed		none	SP
Lascano and Van Bavel (1982)	B H	UCHM	h, T	CD	no	no	no	yes	yes	in situ[5]	RS
Schieldge et al. (1982)	B H	CHM	θ, T	CD DIS	yes	no	no	flux prescribed		in situ[6]	SP
Recan (1982)	B H	CHM	u, T	CD DIS	yes	yes	yes	yes	yes	labo[7]	SP RS
Camillo et al. (1983)	B H	CHM	θ, T	CD DIS	yes	no	no	yes	yes	in situ[8]	RS
Brunet (1984)	B S	CHM	h, T	CD DIS	yes	yes	yes	yes	yes	in situ[9]	SP
Higuchi (1984)	B S	CHM	h, T	CD DIS	yes	yes	no	yes	yes	in situ[10]	SP

(1): B = bare soil; H = homogeneous; V = vegetated; S = stratified.

(2): (a) type of equations considered: coupled (CHM) or uncoupled (UCHM) heat and mass; (b) descriptive variables (see notation); (c) type of heat transport: conductive (CD), convective (CV), distillation (DIS); (d) vapor flow is considered in the mass transfer.

(3): (a) thermal stratifications are considered; (b) interfacial sublayer is considered.

(4): (a) energy balance is considered; (b) radiative balance is considered.

(5): [1]2 days, T_s; [2]several months, T_c; [3]T_s; [4]32 h, 1 profile; [5]1 day, 2 profiles; [6]3 days, 2 profiles; [7]soil column; [8]fitting on T_s; [9]2 days, 1 profile; [10]35 h, 1 profile.

(6): M = meteorology; PP = plant physiology; RS = remote sensing; SP = soil physics.

TABLE 2

Proposed soil heat and mass flow equations

Flux equations	
$q_l = \phi_l\{K_{lh}[(\partial h/\partial z) - 1] + D_{lh}(\partial T/\partial z)\}$	(1)
$q_v = \phi_l\{D_{vh}[\partial h/\partial z] + D_{vt}[\partial T/\partial z]\}$	(2)
$q_m = \phi_l\{D_{lh}[\partial h/\partial z] + D_{lt}[\partial T/\partial z] - K_{lh}$	(3)
$q_h = \delta^*[\partial T/\partial z] - \phi_l\Delta h_v D_{vh}[\partial h/\partial z]$	(4)
Transient flow equations	
$F_1[\partial h/\partial t] + F_2[\partial T/\partial t] = \partial[q_m/\phi_l]/\partial z$	(5)
$C_1[\partial h/\partial t] + C_2[\partial T/\partial t] = \partial[q_h]/\partial z$	(6)
Transport coefficients	
K_{lh} liquid hydraulic conductivity	(7)
$D_{lt} = K_{lh}[\partial h/\partial T]_h$ thermal liquid diffusivity	(8)
$D_{vh} = \phi_l^{-1}\Gamma\mu D_{va}(n - \theta)[\partial\phi_v/\partial T]_T$ isothermal vapor conductivity	(9)
$D_{vt} = \phi_l^{-1}\beta\mu D_{va}[\partial\phi_v/\partial T]_h$ thermal vapor diffusivity	(10)
$D_h = K_{lh} + D_{vh}$ isothermal moisture conductivity	(11)
$D_l = D_{lh} + D_{vt}$ thermal moisture diffusivity	(12)
δ^* apparent thermal conductivity	(13)
Generalized storage coefficients	
$F_1 = [1 - (\phi_v/\phi_l)][\partial\theta/\partial h]_T + [(n - \theta_l)/\phi_l][\partial\phi_v/\partial h]_T$	(14)
$F_2 = [1 - (\phi_v/\phi_l)][\partial\theta/\partial T]_h + [(n - \theta_l)/\phi_l][\partial\phi_v/\partial T]_h$	(15)
$C_1 = (n - \theta_l)\Delta h_v[\partial\phi_v/\partial h]_T - [\phi_l W + \phi_v\Delta h_v][\partial\theta/\partial h]_T$	(16)
$C_2 = C + (n - \theta_l)\Delta h_v[\partial\phi_v/\partial T]_h - [\phi_l W + \phi_v\Delta h_v][\partial\theta/\partial T]_h$	(17)

the soil air phase is continuous and always in connection with constant atmospheric pressure; (H4), in eqn. (*1*)* the transport of absorbed liquid water due to thermal gradients (Kay and Groenevelt, 1974) is neglected; (H5), the vapor movement, eqn. (*2*), is described by a Fickian process and the vapor is a perfect gas; (H6), in eqn. (*3*), no advection of the heat of wetting due to pressure head (Kay and Groenevelt, 1974) is considered; (H7), radiative transfers and convective transport of heat are neglected in eqns. (*4*) and (*6*); for a very permeable soil, convective flux represents at the maximum 8 10% of the conductive one, in very wet conditions (Sophocleous, 1979; Dunand, 1982); (H8), no mass and heat sink terms are considered in the conservation eqns. (*5*) and (*6*); (H9), local thermal equilibrium between solid and fluid phases exists; and (H10), liquid and vapor phases are in local thermodynamical equilibrium; this implies that the vapor specific mass is given by:

$$\phi_v(h, T) = \phi_{va}(T)\exp[M_v g h/RT] \quad (1)$$

It has been shown (Milly, 1982) that these two last assumptions are generally satisfied, except maybe for very high infiltration rates into coarse materials.

* Equation numbers in italics refer to the equations in Tables 2 and 3; equation numbers in normal corps refer to the equations in the text.

It should be noted that the water pressure head (h) is used as the dependent variable instead of either volumetric (Philip and De Vries, 1957; Luikov, 1966; Kay and Groenevelt, 1974; Saugier et al. 1974; Schieldge et al., 1982; Camillo et al., 1983) or gravimetric (Bories et al., 1978; Recan, 1982) water content. This allows the preservation of continuity in passing from unsaturated to saturated zones, or from one layer to another in a layered medium. If needed, the hysteresis effects of the $h(\theta)$ relationship can also be considered (Milly, 1982). The transport and generalized storage coefficients given in Table 2 will be discussed later on in this paper.

Atmosphere equations

To describe the heat and mass transfers in the soil atmosphere continuum, the eqns. (*5*) and (*6*) of Table 2 are coupled with a modeling of the surface boundary layer. The corresponding equations are given in Table 3. They are based on the Prandtl approach and the similarity theory of Monin and Obukhov (1954) to describe the momentum, heat and mass transfers in the lower part of the atmosphere, and on the radiative and energy balances at the soil surface, eqn. (*19*). In the cases of forced and mixed convection (Thom, 1975) the vapor (Φ_v) and sensible (Φ_h) atmospheric fluxes (eqns. (*20*) and (*21*) are expressed in terms of aerodynamic resistances (r_v, r_h) taking into account the thermal stratifications of the atmosphere [eqns. (*24*) and (*25*)] through the integrated stability functions Ω_m, Ω_h, Ω_v which depend on the Monin Obukhov length:

$$L = [\phi_a u_*^3]/[k g(\Phi_h/C_{pa}T_a + 0.61\Phi_v)] \quad (2)$$

The expressions proposed by Paulson (1970) were used. For unstable conditions

TABLE 3

Proposed surface boundary conditions

Continuity equations at $z = 0$	
$q_m = \Phi_v$	(18)
$q_h = R_g(1 - a) - \varepsilon(R_a - \sigma T_a^4) - \Phi_h - \Delta h_v\Phi_v$	(19)
forced convection	
$\Phi_v = (\phi_v|_{z=0} - \phi_{va})/r_v$	(20)
$\Phi_h = \phi_a C_{pa}(T_s - T_a)/r_h$	(21)
free convection	
$\Phi_v = \Phi_h[\varepsilon|_{z=0} - e_a]/[\gamma\Delta h_v(T_s - T_a)]$	(22)
$\Phi_h = -\{[h^*\phi_a C_{pa}(g/T_a)^{1/2}]/[3(z_a^{1/3} - z_{0h}^{1/3})^{3/2}]\}(T_s - T_a)^{3/2}$	(23)
Aerodynamic resistances	
$r_v = \{\mathrm{Ln}[z_a/z_{0v}] - \Omega_v[z_a/L]\}\{\mathrm{Ln}[z_a/z_{0m}] - \Omega_m[z_a/L]\}/(k^2 u_a)$	(24)
$r_h = \{\mathrm{Ln}[z_a/z_{0h}] - \Omega_h[z_a/L]\}\{\mathrm{Ln}[z_a/z_{0m}] - \Omega_m[z_a/L]\}/(k^2 u_a)$	(25)

(L < 0):

$$\Omega_m(x) = 2\,\mathrm{Ln}[(1+x)/2] + \mathrm{Ln}[(1+x^2)/2] - 2\,\mathrm{Arctg}(x) + \pi/2$$

$$\Omega_v(x) = \Omega_h(x) = 2\,\mathrm{Ln}[(1+x^2)/2] \quad (3a)$$

where (x) stands for $[1 - 16(z/L)]^{1/4}$. For stable situations (L > 0):

$$\Omega_m(x) = \Omega_v(x) = \Omega_h(x) = -5(z/L), \quad \text{for } (z/L) \leq 1$$

$$\Omega_m(x) = \Omega_v(x) = \Omega_h(x) = -5.[1 + \mathrm{Ln}(z/L)], \quad \text{for } (z/L) > 1 \quad (3b)$$

For free convection conditions Φ_h was estimated by the Priestley formulation (1959) with $h^* = 1.27$, eqn. (*23*), and Φ_v was expressed as a function of Φ_h through the Bowen ratio, eqn. (*22*) calculated between the soil surface and the reference level.

It should be mentioned that, unlike most of the models available in the literature, different roughness lengths for water vapor (z_{0v}), sensible heat (z_{0h}) and momentum (z_{0m}) have been considered in eqns. (*24*) and (*25*).

As a matter of fact, the study conducted by Recan (1982) clearly showed that surface temperature estimates are much more sensitive to uncertainties on z_{0m} if z_{0m}, z_{0v} and z_{0h} are assumed to be the same, instead of different as they should be from the theoretical viewpoint when the transfers in the viscous boundary sublayer are considered. The relations given by Brutsaert (1975) have been used:

$$\left.\begin{aligned} z_{0h}/z_{0m} &= 0.624/Re^* \\ z_{0v}/z_{0m} &= 0.395/Re^* \end{aligned}\right\} \text{ for } Re^* < 0.13 \quad (4a)$$

$$\left.\begin{aligned} z_{0h}/z_{0m} &= 7.4\exp[-2.46\,Re^{*0.25}] \\ z_{0v}/z_{0m} &= 7.4\exp[-2.25\,Re^*] \end{aligned}\right\} \text{ for } Re^* > 2 \quad (4b)$$

where $Re^* = u_* z_{0m}/\mu$ is the roughness Reynolds number. Due to the lack of a model for the transitional regime from smooth ($Re^* < 0.13$) to rough ($Re^* > 2$) flow, an interpolation between eqn. (4a) and (4b) was applied to estimate z_{0h} and

MATERIALS AND METHODS

Experimental set-up

An experiment was conducted on a 3600 m² (60 × 60 m) bare plot located at the INRA Research Station located at Montfavet (France). The plot was selected on a larger field (10,000 m²) in order to minimize lateral advective atmospheric effects. Due to possible spatial variations of the soil properties, the plot was preliminarily surveyed at 52 points located at 10 × 10 m equilateral grid nodes (Fig. 1). At each point, some classical soil properties (textural components, bulk density) were determined. Based on statistical and geostatis-

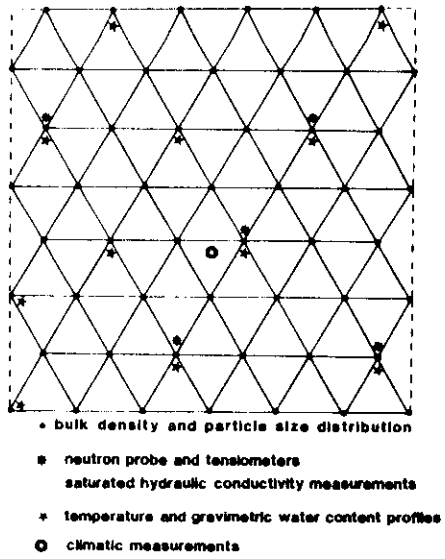

Fig. 1. Experimental set-up.

tical analysis five sites (Fig. 1) were chosen and equipped with a neutron access tube (80 cm depth) and five tensiometers (15, 30, 45, 60 and 80 cm) connected with mercury manometers in order to measure the time evolution of moisture content and hydraulic head profiles and to estimate the components of the soil water balance.

Twelve sites (Fig. 1) were provided with thermal probes horizontally installed at 1, 2, 6, 11, and 26 cm depth to measure the time evolution of temperature profiles and to infer the in-situ thermal basic properties. Every day, soil samples up to 30 cm deep were taken close to the probes in order to determine soil moisture profiles, the gravimetric water content measurements being converted into volumetric water content values through the corresponding bulk densities. A micrometeorological mast installed near the center of the plot (Fig. 1) was equipped with appropriate sensors at four levels (38, 54, 92 and 128 cm high) to measure wind velocity, temperature and vapor pressure profiles in the air. Incident and reflected solar radiations as well as net and atmospheric ones were also recorded. All these allowed to determine the surface parameters (albedo and aerodynamic roughness length) and the atmospheric fluxes Φ_h and Φ_v which were considered as representative of the whole field. All the data were automatically recorded on a 30 min basis, except the neutron probe and tensiometer readings (daily measurements).

The plot, including the border zone, was sprinkler irrigated (26.5 mm) and the subsequent drying was studied during a one week period.

Soil properties

Textural and structural properties

Table 4 summarizes the main results dealing with the textural components and bulk density determined at the 52 points of the grid and within the first 30 cm of soil. Figure 2 gives the mean dry bulk density profile, as well as the associated standard deviations. The values were obtained using a gamma transmission probe (Bertuzzi et al., 1987). Note that in the first 30 cm, 52 spatial replications per depth were performed, whereas only five replications per depth were obtained for the deeper layers. The main comments can be made:

(1) All the observations taken in the first 30 cm of soil were found to be normally distributed with small coefficients of variation ($CV < 8\%$).

(2) Both the visual inspection of the soil surface and the analysis of the bulk density profiles (Fig. 2) showed that three layers should be considered: the first one about 5 mm thick corresponds to a crust induced by interactions between the soil structure and both rainfall and previous irrigation applications. The dry bulk density was estimated at approximately 1.45 g cm $^{-3}$. The second one (0.5–30 cm) is quite homogeneous (1.32 ± 0.04 g cm $^{-3}$) and the third one (30–80 cm) appears more compacted (1.54 ± 0.05 g cm $^{-3}$).

(3) The experimental semi-variograms given in Fig. 3 show that for the sampling distances considered, the bulk density observations were completely randomly distributed (Fig. 3b) and the percentages of particles smaller than 20 μm (clay plus silt) appeared to be correlated up to a distance of about 20 m (Fig. 3a). Directional semi-variograms did not show any significant anisotropy.

Based on these results, the five measurement sites of the water balance components (see Fig. 1) were chosen in such a way that, first, they may be considered as mutually independent (minimum distance of 20 m) and, second, they were located at particular points of the "clay plus silt" probability density function (namely the mean value ± 1 or 2 standard deviations). By making this choice, it was implicitly assumed that the variability of the "clay plus silt" content would be the most important factor responsible of the spatial variations of the water content profiles themselves.

TABLE 4

Main soil characteristics of the three layers

	Soil layers		
	Crust	0.5–30 cm	30–80 cm
Bulk density (g cm $^{-3}$)	1.45	1.32 ± 0.04	1.54 ± 0.05
Porosity	0.45	0.50	0.42
Clay content (%)		27.2 ± 1.08	
Silt content (%)		61.7 ± 1.1	
Sand content (%)		11.0 ± 0.9	
Organic matter (%)		1.70 ± 0.08	
K_s (m s $^{-1}$)	$2.8 \times 10^{-6} \pm 3.0 \times 10^{-6}$	$1.3 \times 10^{-4} \pm 1.4 \times 10^{-4}$	$9.6 \times 10^{-6} \pm 1.0 \times 10^{-5}$

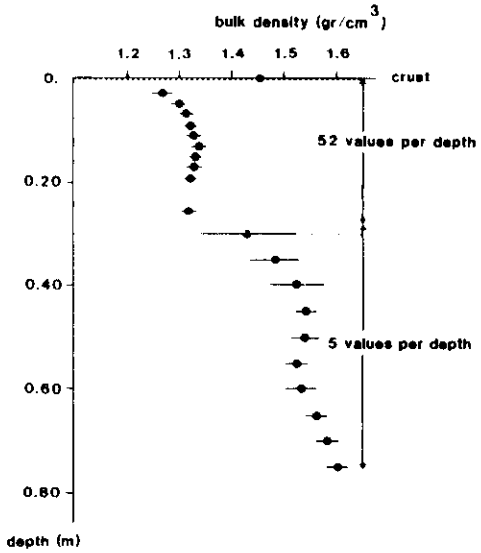

Fig. 2. Dry bulk density profile. The horizontal bars correspond to ± one standard deviation.

Hydrodynamic properties

(1) The water potential–water content relationships were obtained by using both the neutron probe and tensiometer data, and by making laboratory measurements [Richards pressure plate apparatus on the range 0 to −165 m of water and vapor pressure equilibrium technique for dryer conditions] on disturbed soil aggregates taken in the upper 30 cm of the soil profile. For this layer, a good agreement can be observed (Fig. 4) between laboratory and field determinations in the working range of tensiometers. The differences between the field measurements in the 0.5–30 cm and 30–80 cm layers may be attributed to changes in the textural composition. Table 5 gives the results obtained by the pressure plate and saline solution techniques performed on soil samples taken in the 0.5–30 cm layer. These values were assumed to be the same for the other layers. All the gravimetric water content values measured on disturbed samples were converted into volumetric ones by the appropriate bulk density values of each layer of soil.

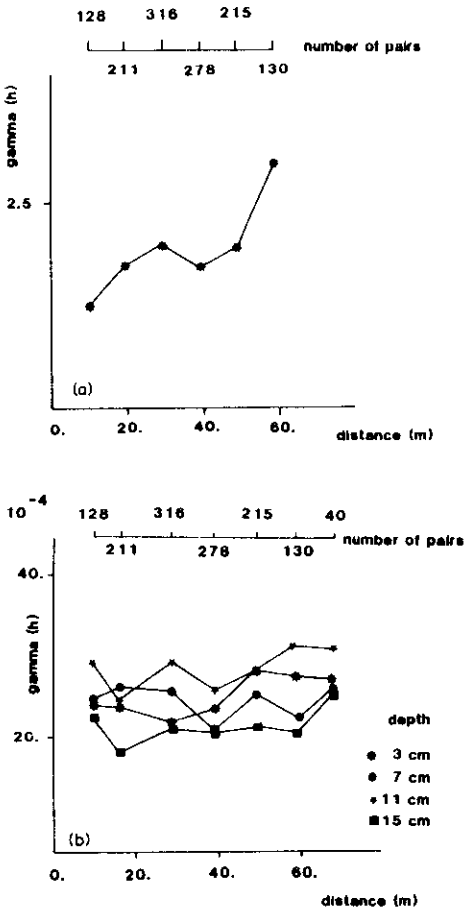

Fig. 3. Experimental semivariograms of the "silt + clay" contents (a) and the dry bulk density (b) measured at the 52 points.

(2) The liquid hydraulic conductivity was estimated by Mualem's model (1976):

$$K_{1h} = K_s S^p \left(\left\{ \int_0^{\theta} |d\theta/h(\theta)| \right\} \Big/ \left\{ \int_0^{\theta_s} |d\theta/h(\theta)| \right\} \right)^2 \quad (5)$$

where $S = (\theta - \theta_r)/(\theta_s - \theta_r)$, p is a fitting parameter (based on statistical analysis, Mualem proposed $p = 0.5$ with values ranging from -2.0 to 2.5) and K_s is the saturated hydraulic conductivity. While for each layer the water potential–water content relation was known; (p) was considered as a fitting

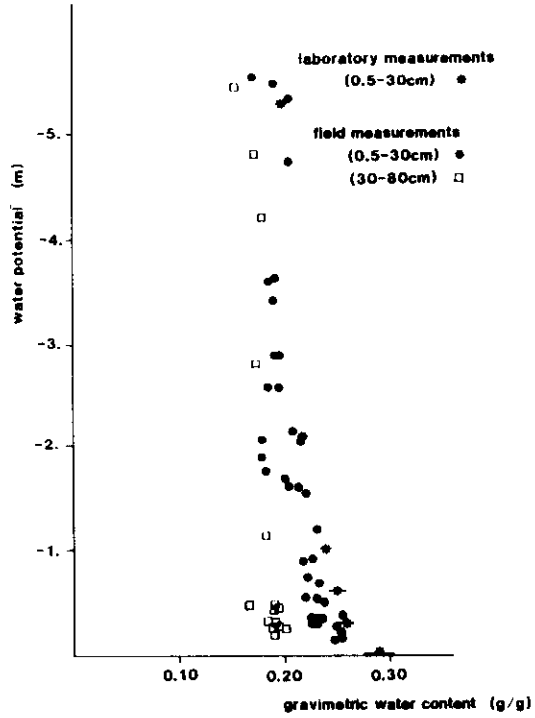

Fig. 4. Water potential as function of gravimetric water content.

parameter, and K_s was measured on undisturbed soil samples taken in the top (0.5–30 cm) and deep (30–80 cm) layers (twelve replicates per layer) and by using the local trickle irrigation technique (Boiffin, 1984) for the crust (twelve spatial replications). The results are reported in Table 4. For the crust, it should be mentioned that the measurement of the steady-state infiltration regime close to saturation leads to overestimations of K_s (Lafolie and Bruckler, 1988). As can be expected from many other experimental studies, the variability of the observations of K_s both in the horizontal plane and the vertical direction is very high ($CV \approx 100\%$). It includes both local experimental uncertainties and spatial variations themselves.

The temperature dependence of K_{1h} was only considered through the kinematic viscosity $\mu(T)$:

$$K_s(T) = K_s(T_0)\, \mu(T_0)/\mu(T) \quad (6)$$

with $T_0 = 20°C$.

(3) The thermal liquid diffusivity was estimated by eqn. (*8*) in Table 2 with

TABLE 5

Water potential as function of gravimetric water content determined by the pressure plate and saline solution techniques

Water potential (m)	Replicates	Gravimetric water content	
		Mean	Standard deviation
Pressure plate			
1	25	0.239	0.005
5	25	0.198	0.004
10	15	0.176	0.003
38	10	0.141	0.004
82	10	0.130	0.003
165	10	0.097	0.004
Vapor equilibrium			
335	3	0.070	0.003
780	3	0.044	0.002
1485	3	0.034	0.002
2692	3	0.032	0.001
6577	3	0.021	0.001
12196	3	0.017	0.000

$[\partial h/\partial T]_h] = -6.8 \times 10^{-3} h$. Because of great experimental uncertainties and controversial results reported in the literature about the temperature dependence of $h(\theta)$ (Bories et al., 1978; Constantz, 1982; Nimmo and Miller, 1986), we have adopted here a coefficient which is over three times the value ($-2 \times 10^{-3} K^{-1}$) predicted by the classical surface tension model (Philip and De Vries, 1957).

(4) Isothermal and thermal vapor transport coefficients were estimated by the Philip and De Vries model (1957) [eqns. (*9*) and (*10*) in Table 2] where the molecular diffusivity of water vapor in the air is given by:

$$D_{va} = 2.29 \times 10^{-5}[1 + (T/273.16)]^{1.75} \quad (m^2 s^{-1}) \qquad (7)$$

and the derivatives $[\partial \phi_v/\partial h]$ and $[\partial \phi_v/\partial T]$ can be calculated from eqn. (1) in the text.

In eqn. (*9*), the tortuosity of the air-filled pore domain was expressed as (Lai et al., 1976): $\Gamma = (n - \theta)^{2/3}$

In eqn. (*10*), the enhancement factor β was estimated as (Jury and Letey, 1979):

$$\beta = f(\theta_a) f r \qquad (8)$$

with:

$$f(\theta_a) = \theta_a[1 + \theta/\theta_{ak}], \quad \text{for } \theta_a < \theta_{ak}$$

$$f(\theta_a) = n, \quad \text{for } \theta_a \geq \theta_{ak}$$

$$f = \{[1 + \theta/\theta_{ak}]/[1 - (\theta/\theta_{ak})(\delta_v/\delta_l)]\}^2$$

and r is the ratio of the volume averaged temperature gradient of the entire medium. It has been calculated by the model given by Milly (1984).

Thermal properties

(1) The volumetric heat capacity of the soil was calculated as a weighted average of the capacities of its components (quartz, other minerals, organic matter, air and liquid water).

(2) The heat of wetting in the eqns. (*16*) and (*17*) in Table 2 was classically (De Vries, 1958) estimated by:

$$W = j^{-1} g T[(\partial h/\partial T) - (h/T)] \qquad (9)$$

(3) The apparent thermal conductivity of the upper layer (0.5–30 cm) was obtained through the estimation of $C(\theta)$ and field determination of the thermal diffusivity $\alpha^*(\theta)$. This was done by analysing the measured temperature profiles and by solving the linearized heat conduction equation (on a daily basis) by a convolution product method modified to account for non uniform initial profiles (Passerat de Silans, 1986). The results obtained at twelve locations (see Fig. 1) are presented in Fig. 5. The dispersion of the values is represented by horizontal and vertical bars. Some values determined on disturbed soil samples compacted at different dry bulk densities in a conductivymeter, by using a numerical finite element method fitted on temperature measurements (Bruckler et al., 1987) are also reported in Fig. 5.

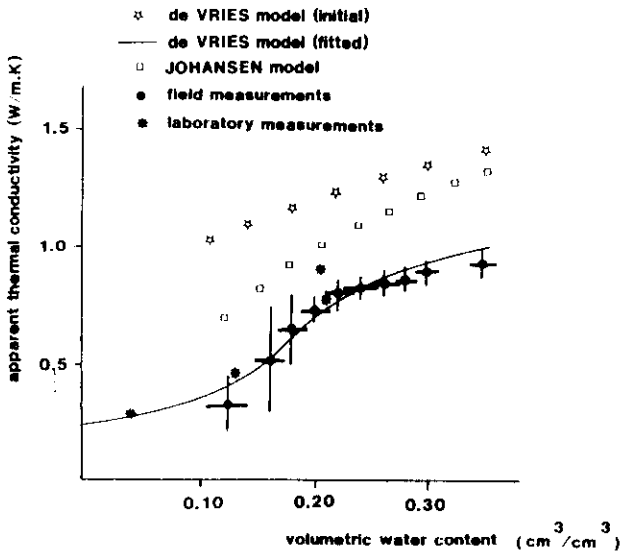

Fig. 5. Apparent thermal conductivity as function of volumetric water content for the second layer (0.5–30 cm).

For comparison purposes, the theoretical calculations proposed by De Vries (1966) and Johansen (1975) are also given. It appears that such models, often extensively used by many authors cannot be applied in confidence without a fitting procedure, at least. For instance, by adjusting the shape factors of quartz and other minerals (0.200 instead of 0.125 in the De Vries model) and considering the temperature dependence of the thermal conductivity of the air-filled pores, as proposed by Cary (1979), a good agreement may be obtained between theoretical estimations of the thermal conductivities and laboratory as well as field determinations. The fitted De Vries model was assumed to be applicable for the three layers, without any further modification.

Surface properties

(1) The measurements of incident and reflected solar radiations provided experimental values of the albedo. An example is given in Fig. 6a for three different days during the experimentation. By eliminating the solar angle effect (Bartman, 1980) the normalized albedo values as a function of the volumetric water contents measured on the first 0.5 cm divided by the porosity are presented in Fig. 6b. The following expression was fitted on these values:

$$\left.\begin{aligned} a &= 0.40 - 0.32[\theta/n], \quad \text{for } |\theta/n| < 0.5 \\ a &= 0.24, \quad \text{for } |\theta/n| \geqslant 0.5 \end{aligned}\right| \quad (10)$$

(2) According to the expression proposed by Sellers (1965) the surface emissivity was estimated as:

$$\varepsilon = 0.90 + 0.18\theta \quad (11)$$

(3) The aerodynamic roughness length was determined by analyzing the wind speed profiles corresponding to both neutral and stable situations (Saugier, 1974). Figure 7 shows the relation between z_{0m} and the roughness Reynolds number. For $Re^* > 1.7$, the roughness length was assumed to be constant and the mean value is $z_{0m} = 1.75 \times 10^{-4}$ m. This small value appears to be in good agreement with the flat and smooth characteristic of the soil surface. For $Re^* < 1.7$ the dependence of z_{0m} on Re^* was taken into account through the following fitted expression:

$$z_{0m} = 1.06 \times 10^{-4} Re^{*0.924} \quad (12)$$

The roughness lengths for vapor and sensible heat were then estimated by the eqns. (4a) and (4b) in the text.

NUMERICAL MODEL

Soil

The nonlinear parabolic partial differential eqns. (5) and (6) which are of identical forms were solved by a Galerkin finite element method with N linear

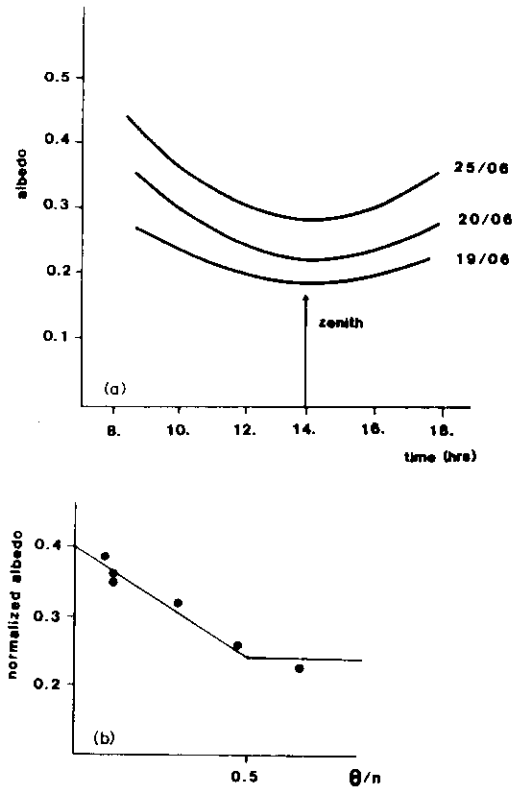

Fig. 6. Smoothed albedo measurements as function of time for 3 days (a) and normalized albedo as function of water content of the crust (b).

elements of variable length increasing from 0.2 cm at the surface to 10 cm at the bottom of the profile ($z = 80$ cm). Time integration was achieved by the Crank–Nicolson method with a time step automatically varying from 30 s to 400 s according to the magnitude of the state variable changes. The resulting linear system ($2N \times 2N$ equations) was solved by the Thomas algorithm (see Remson et al., 1971). More details as well as the computer code are given in Passerat de Silans (1986).

Because no analytical solutions are available for this complicated problem, the calculated solutions have been compared with known analytical or quasi-analytical solutions of different problems, each designed to test a particular feature of the model and more precisely of mutually independent heat and mass flows.

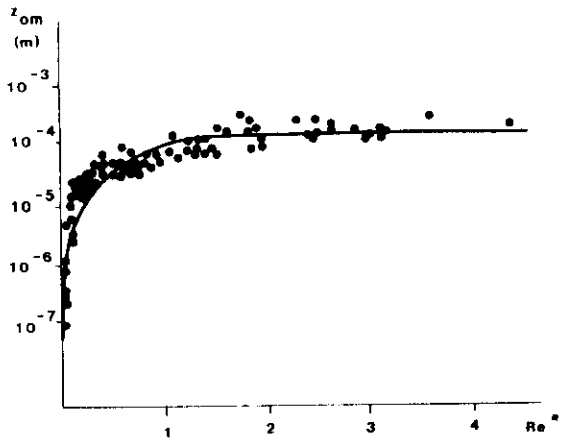

Fig. 7. Aerodynamic roughness length as function of roughness Reynolds number.

Example 1

The problem of pure heat conduction transport in a homogeneous semi-infinite medium (eqn. (6) with $C_1 = 0$, $C_2 = C$, and $q_h = -\delta^*|\partial T/\partial z|$) was solved for the following initial and boundary conditions:

$$z \geq 0, \quad t < 0, \quad T(z) = T_i = 293 \text{ K} \tag{13a}$$

$$z = 0, \quad t \geq 0, \quad q_h = h_c|T_a - T_s| \tag{13b}$$

with $h_c = 10\,\text{W m}^{-2}\text{K}^{-1}$, and $T_a = 305$ K

The corresponding analytical solution is available in Carslaw and Jaeger (1959):

$$(T - T_i)/(T_a - T_i) = 1 - \text{erf}a^* - \{\exp[(h_c z/\delta^*) + (h_c^2 \alpha^* t/\delta^{*2})]\} \times \{1 - \text{erf}[a^* + (h_c(\alpha^* t)^{1/2}/\delta^*)]\} \tag{14}$$

with $a^* = z/(4\alpha^* t)^{1/2}$.

Numerical results obtained by the model run with $N = 50$ elements of equal length (1 cm) and constant time step (10 s) are presented in Fig. 8. They agree very well with the analytical solution, the difference being less than 0.1 K. Note that the calculations were made with $\alpha^* = 10^{-6}\,\text{m}^2\text{s}^{-1}$ and $\delta^* = 2\,\text{W m}^{-1}\text{K}^{-1}$.

Example 2

The problem of isothermal water infiltration under constant flux applied to the soil surface has been considered. It is described by the eqn. (5) of Table 2 with $F_1 = \partial\theta/\partial h$, $F_2 = 0$ and $q_m = -\phi_1 K_{lh}[(\partial h/\partial z) - 1]$ associated with the following initial and boundary conditions:

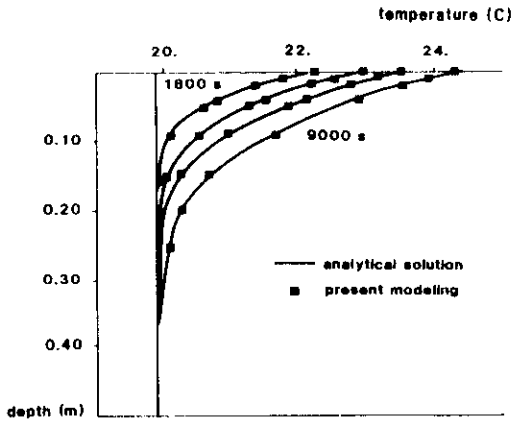

Fig. 8. Solutions of the heat linear conduction equation with radiative condition at the surface.

$$z \geq 0, \quad t < 0, \quad h(z) = h_i(z) \tag{15a}$$

$$z = 0, \quad t \geq 0, \quad -K_{lh}[(\partial h/\partial z) - 1] = q_0 \tag{15b}$$

This problem has been solved by Boulier et al. (1984) by using a quasi-analytical procedure based on the flux-concentration approach which was checked against both numerical solution of the Richards equation (finite difference scheme) and experimental values obtained on a soil column. As shown by Fig. 9, a good agreement can be observed between these results and the present model run by using $N = 40$ elements of 1 cm long and a time step of 1 s. Having established the validity of the model for simulating different simple and uncoupled processes, it has been assumed that it may be used with confidence for more complicated situations involving coupled phenomena.

Soil atmosphere interface

Solving the soil model requires at each time-step the knowledge of the surface boundary conditions given by eqns. (*18*) and (*19*) which can be expressed as:

$$-\phi_l\{D_{lh}[\partial h/\partial z] + D_{lt}[\partial T/\partial z] - K_{lh}\}_{z=0} = \Phi_v \tag{16a}$$

$$\delta^*|\partial T/\partial z| + \phi_l \Delta h_v D_{vh}[\partial h/\partial z] = R_g(1 - a) + \varepsilon(R_a - \sigma T_s^4) + \Phi_h + \Delta h_v \Phi_v \tag{16b}$$

where Φ_v and Φ_h given by eqns. (*20*) or (*22*) and by eqns. (*21*) or (*23*) respectively (Table 3) are functions of both the surface temperature T_s and the surface water pressure h_s related to ϕ_v through eqn. (1) of the text.

By expressing the gradients $(\partial T/\partial z)$ and $(\partial h/\partial z)$ at $z = 0$ by $(\partial T/\partial z)$

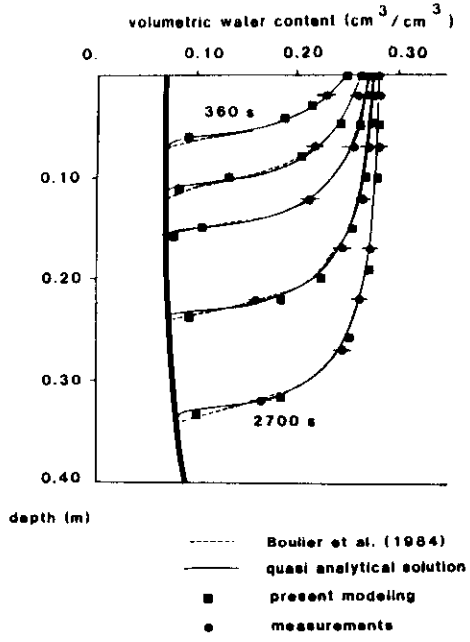

Fig. 9. Isothermal infiltration with constant flux at the surface (Boulier et al., 1984).

$(T_2 - T_s)/\delta z_2$ and $(\partial h/\partial z) = (h_2 - h_s)/\delta z_2$ where T_2 and h_2 are the values of temperature and water pressure at $z_2 = \delta z_2$ the above eqns. (16a) and (16b) take the following general form:

$$f_1(T_s, h_s) = 0 \quad (17a)$$

$$f_2(T_s, h_s) = 0 \quad (17b)$$

This nonlinear system has been solved by using the steepest descent method which minimizes the functional $f = f_1^2 + f_2^2$. At each time-step of calculation, initial values $(T_{s_j}(0); h_{s_j}(0))$ of the iterative process correspond to extrapolated ones from the two previous time steps $(T_{s_{j-1}}; T_{s_{j-2}}; h_{s_{j-1}}; h_{s_{j-2}})$. At each iteration, a test on the Monin Obukhov length is performed in order to express Φ_h and Φ_v accordingly. The rate of convergence of the iterative procedure is increased by using the Aitken formula (for further details, see Passerat de Silans, 1986).

NUMERICAL VERSUS EXPERIMENTAL RESULTS

The model previously described was run with the measured input variables (u_a, T_a, e_a at $z_a = 1.28$ m, R_a, R_g).

All the experimental records are given in Fig. 10. Dirichlet conditions

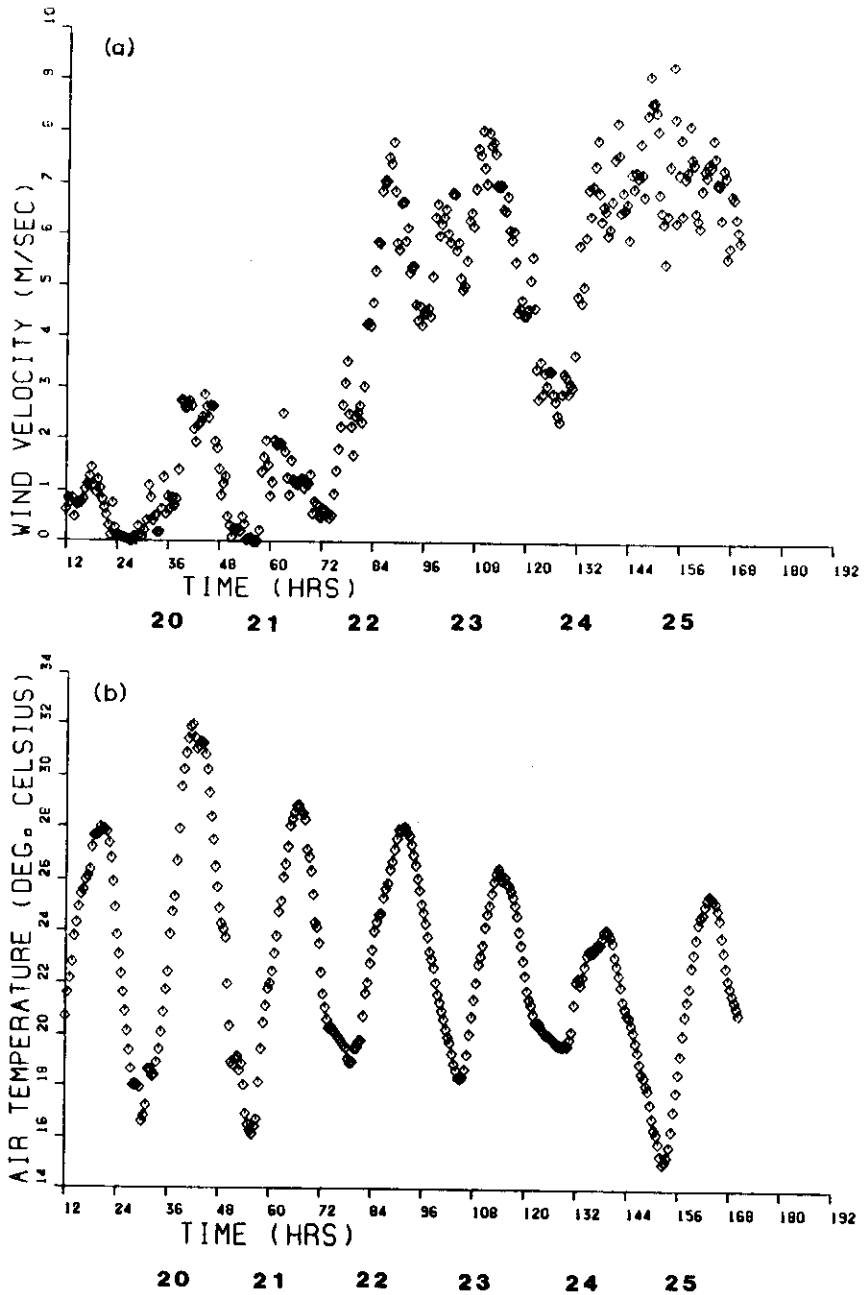

Fig. 10. Measured time evolutions of input variables: wind velocity (a); air temperature (b); vapor pressure (c) at 1.28 m height; global and atmospheric radiations (d).

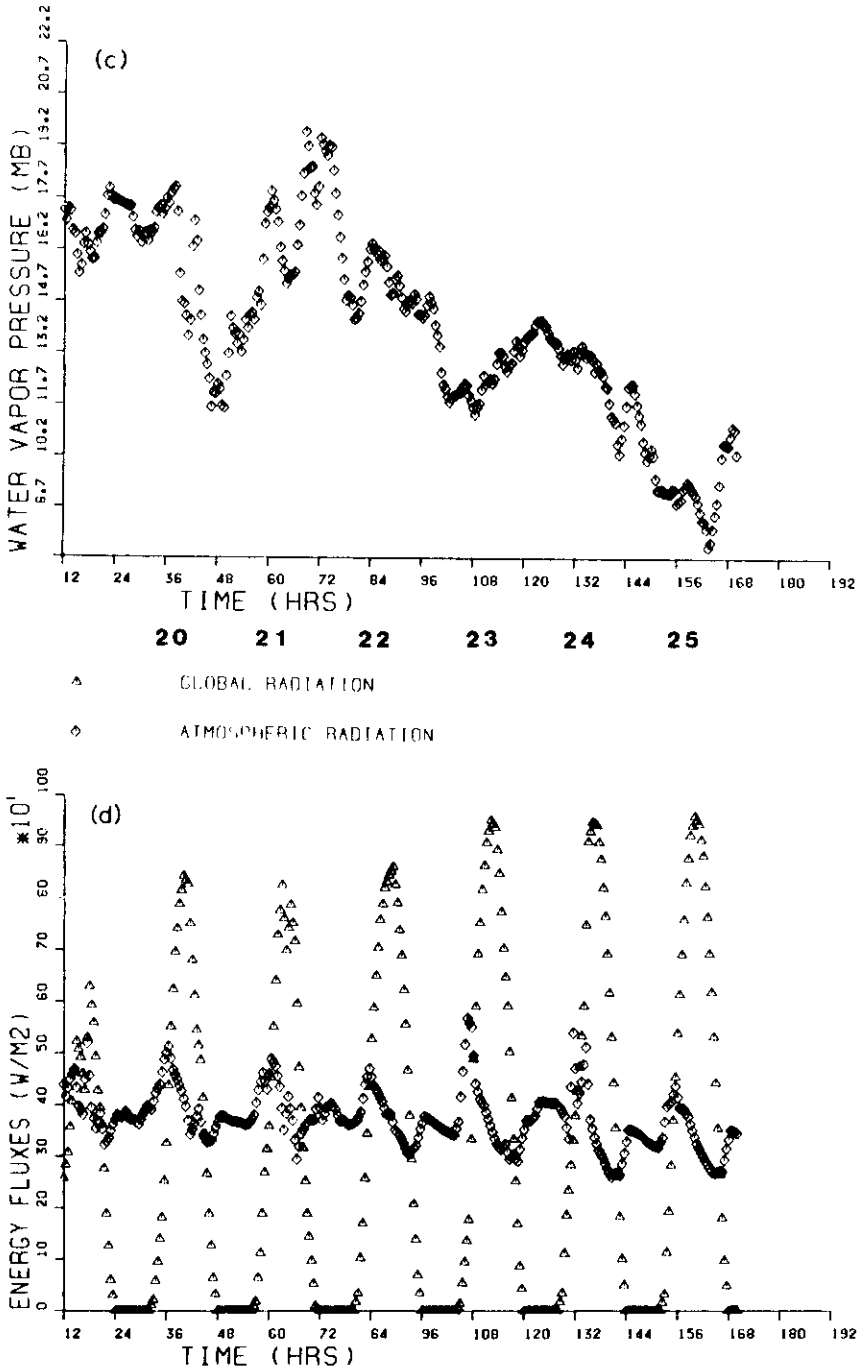

(h_L = −40 cm of water and T_L = 20°C) were imposed at the bottom (z_L = 80 cm) of the soil profile.

Because of uncertainties in some parameters and lack of experimental determination of the unsaturated soil hydraulic conductivity, the model was first fitted on the soil water content and temperature time evolutions measured on the period June 19, 11 h–June 21, 17 h and then evaluated by comparing observations and calculations on the June 21, 17 h June 25, 15 h period.

Calibration phase

A sensitivity analysis previously conducted having shown that the parameters (K_s, p) describing the unsaturated hydraulic conductivity were among the most sensitive ones especially for wet conditions, only these parameters were adjusted by best fitting between observations and numerical calculations. The best results given in Fig. 11 were obtained with $K_s = 1.4 \times 10^{-7}$ m s^{-1} and $p = 7$ for the intermediate layer, the difference

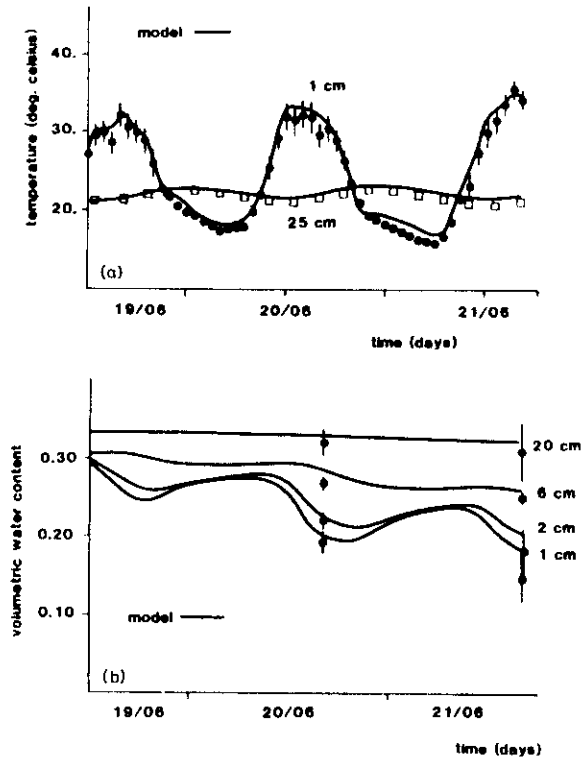

Fig. 11. Calibration of the model: comparison between observed and fitted time evolutions of soil temperature (a); and volumetric water content (b). The vertical bars correspond to ± one standard deviation of the measurements.

between observed and calculated values being less than 2°C (Fig. 11a) and 0.02 $cm^3 cm^{-3}$ (Fig. 11b). Note that the experimental time evolutions of both soil water content and temperature at different depths, as well as initial profiles were taken as the spatial average of the observations.

Validation phase

The numerical model was then used to simulate the evolutions of the temperature and the water content soil profiles along the period June 21 June 25. As an example, Fig. 12 shows the observed and computed temperature (Fig. 12a) and volumetric water content (Fig. 12b) variations at different depths. The model describes quite well short and long time variations of both the temperature and moisture. Nocturnal rewetting of the surface layers is visible in Fig. 12b especially on June 22–23. A good agreement between simulated and observed values can be seen, except for the water content at $z = 1$ cm. This may be explained by the formation of small cracks, observed at the soil surface during the drying process, probably invalidating some basic assumptions of the model such as H1, H7, and H10.

Figure 13 presents the computed cumulative evaporation as function of time as well as field determinations obtained by the zero mass flux plane method (Vachaud et al., 1978) applied to neutron and tensiometer readings at the five sites. The Penman potential evaporation is also given. Figure 14 shows the time evolution of the zero-mass-flux plane depth calculated by the model and experimentally determined by the tensiometer readings.

Table 6 presents the comparison between calculated and measured daily values of the evaporation as well as the Penman estimates. Note that the atmospheric fluxes were obtained on a 30 min basis by the combined aerodynamic method, and integrated over the period specified in Table 6. The corresponding values are considered as representative of the whole field. The soil fluxes estimated by the soil water balance method correspond to the average of the results obtained at the five sites of measurements. The associated standard deviations are also reported in Table 6. The results suggest the following comments:

(1) Taking into account the observed spatial variability of soil measurements, a very fair agreement exists between simulated and experimental values of the time evolution of the cumulative evaporation (Fig. 13 and Table 6) and the zero-flux plane depth. However it appears that the model tends to overestimate the evaporation as the soil becomes drier and drier. A detailed analysis reveals that the model predicts relatively high evaporation rates during the last three nights (3.9 mm in overall). This is in agreement with the calculated temperature patterns (Fig. 12a) which are underestimated as compared to the experimental ones. Because the Penman values have confirmed the high climatic evaporative demand, this behavior has been attributed to the hydraulic and thermal functioning of the cracks which offer additional resistances to the evaporation process and probably limit the night-time rewetting phenomena.

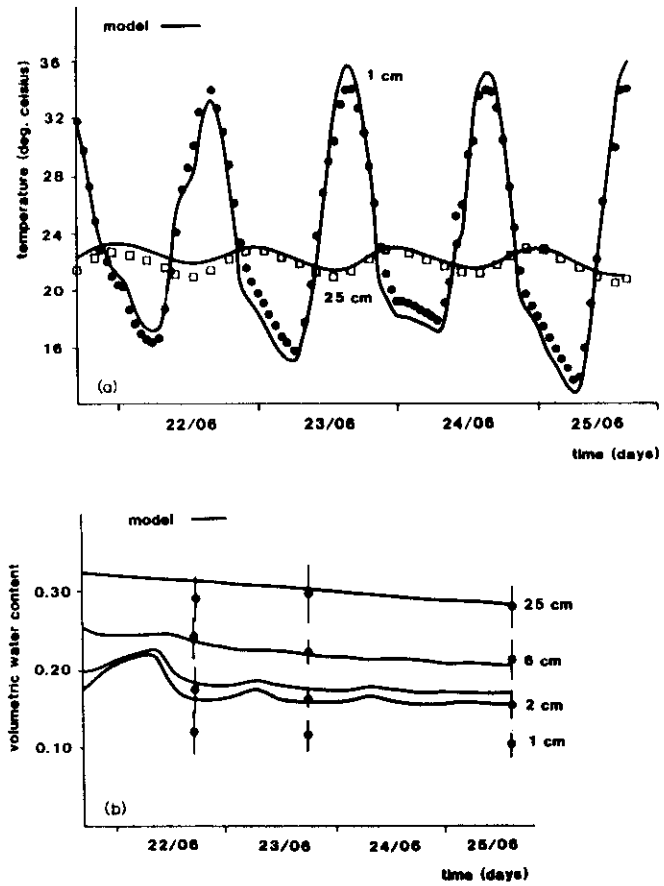

Fig. 12. Evaluation of the model: comparison between observed and calculated time-evolutions of soil temperature (a) and volumetric water content (b).

(2) While the model has been calibrated on the time evolutions of the soil water content and temperature, measured over the period June 19–21 the good agreement between observed and calculated values of the evaporation and the zero-flux plane depth on the same period may be interpreted as an additional test of the validity of the fitting procedure even if the uniqueness of the solution cannot be demonstrated.

(3) The influence of the soil resistance on the evaporation becomes significant on the third day after the irrigation and this also corresponds to a color

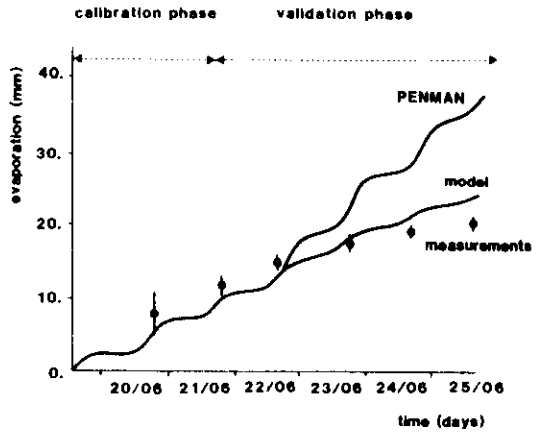

Fig. 13. Comparison between measured and calculated cumulative evaporation. The vertical bars correspond to ± one standard deviation of the measurements.

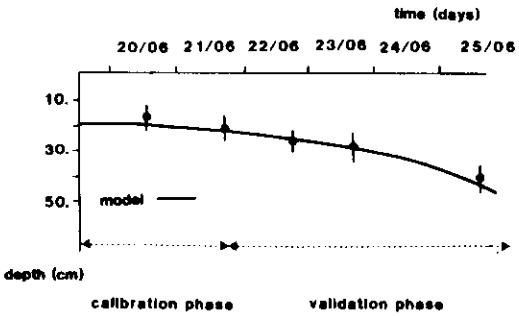

Fig. 14. Comparison between measured and calculated time evolution of the zero-mass-flux plane depth. The vertical bars correspond to ± one standard deviation of five measurements.

change visually observed at the soil surface and confirmed by the albedo measurements. This behavior well agrees with the results reported by Idso et al. (1974) for the Avondale loam soil of similar texture as this one.

(4) Table 6 shows a very acceptable agreement between the daily values of evaporation estimated by either atmospheric or soil measurements considering the degree of accuracy which can be expected by the former method (about 20% according to Saugier and Ripley, 1978) and the soil spatial variations in the latter one. With this respect, the large standard deviations observed the first two days are explained by the non-uniformity of the irrigation.

TABLE 6

Daily values of actual evaporation (mm) estimated by atmospheric and soil measurements, calculated by the model, and potential evaporation using Penman's formula (the values in column 3 represent the average and the standard deviation of the five measurement sites)

Period	Atmospheric flux	Soil flux	Model	Penman
19 (11 h) 20 (17 h)	5.2	7.9 ± 2.8	5.6	5.6
20 21	3.0	4.2 ± 1.2	4.3	4.3
21 22	2.7	2.6 ± 0.7	4.2	6.4
22 23	2.9	2.5 ± 0.9	4.2	8.5
23 24	2.2	1.7 ± 0.4	3.3	7.5
24 25 (15 h)	1.9	1.3 ± 0.4	2.9	7.7
Total (mm)	17.9	20.2	24.5	40.0

SUMMARY AND CONCLUSIONS

A numerical model of soil and atmospheric surface boundary layers is presented, which simulates coupled heat and water movements. It is based on the Philip and De Vries formalism (1957) modified by Milly (1982) for the soil heat and water flows in the soil. Temperature and water pressure head are used as the descriptive variables. The surface boundary layer is modeled by the Prandtl approach and the similarity theory of Monin and Obukhov (1954), taking into account the thermal stratifications of the lower part of the atmosphere, with inclusion of the viscous boundary sublayer leading to different roughness lengths for water vapor, sensible heat and momentum transports. The model is driven by surface energy and mass balance equations estimated by meteorological data (wind velocity, air temperature, vapor pressure, solar and atmospheric radiations). The numerical results obtained by a Galerkin finite element method are compared with field data measured on a 3600 m^2 bare soil exhibiting three different horizons on the first 80 cm including a crust 5 mm thick at the surface. The experimentations as well as the simulation were carried out during a period of seven days following a sprinkler irrigation.

The model is first calibrated on the first two days by fitting the calculated time evolutions of soil temperature and water content at different depths to the observed ones and then evaluated on the following five days by confronting computed and measured soil thermal and hydraulic fields as well as evaporation fluxes. The main features are as follows:

(1) The model describes quite well short and long time variations of soil temperature and water content at different depths and a very fair agreement between predicted and observed values is shown, the difference being less than 2°C and 0.02 $cm^3 cm^{-3}$ respectively.

(2) Taking into consideration the accuracy which can be expected on the estimation of evaporation fluxes from the flux-profile relationships over the surface (about 15–20%) and the spatial variations of the measured soil water

balance components (CV = 25%), the calculated evaporation values agree quite well with the observed ones, all of them becoming significantly smaller than the Penman estimates, the third day following the irrigation.

(3) As the soil becomes drier and drier, the cracks appearing at the surface invalidate some basic assumptions of the model and this may explain the differences between calculated and measured values which are observed at the end of the simulation period.

(4) The large number of parameters, the experimental uncertainties on the estimation of some of them (i.e. soil hydraulic properties) and the difficulty to determine some others (i.e. vapor flow coefficients) require the model to be calibrated. For the situation encountered in the experiment, hydraulic conductivities of the first two layers of the soil and especially of the crust are found to be the most sensitive parameters to be fitted.

(5) Laboratory and field determinations of the apparent thermal conductivity as function of volumetric water content show that theoretical models cannot be straightforwardly used without a calibration at least. The same conclusion applies to Mualem's model (1976) to estimate unsaturated hydraulic conductivity from the soil water retention curve.

(6) Because the soil variability in its horizontal extension is relatively small as compared to the vertical one, an approach able to model only deterministic heterogeneities is considered. In case of more heterogeneous soils, a stochastic approach would be probably more appropriate.

Because the model requires the knowledge of numerous parameters, many of them being not easily obtainable, it may be viewed as too sophisticated for applied research. However, based on the results, it may be thought that it can be considered as a reference model which could be used to evaluate simplified approaches depending on the practical problem to be solved.

ACKNOWLEDGEMENTS

The authors are grateful to P. Bertuzzi and J.C. Gaudu for their helpful assistance in the field experiment and data analysis.

REFERENCES

Bartman, F.L., 1980. A time variable model of earth's albedo. NASA Rep. 159.

Bertuzzi, P., Bruckler, L., Gabilly, Y. and Gaudu, J.C., 1987. Calibration, field testing and error analysis of a gamma-ray probe for the in-situ measurement of dry bulk density. Soil Sci., 144(6): 425–436.

Boiffin, J., 1984. Dégradation structurale des couches superficielles du sol sous l'action des pluies. Thèse de Doctorat de l'Institut National Agronomique Paris-Grignon.

Bories, S., Crausse, P. and Bacon, G., 1978. Etude expérimentale et simulation numérique des transferts de chaleur et de masse en milieu poreux. 6th Int. Transfer Conf. Toronto, Proc., 1: 317 321.

Boulier, J.F., Touma, J. and Vauclin, M., 1984. Flux-concentration relation-based solution of constant flux infiltration equation. Soil Sci. Soc. Am., J., 48: 245–251.

Bruckler, L., Renault, P. and Aries, F., 1987. Laboratory estimation of apparent soil thermal conductivity using a numerical approach. Soil Sci., 143(6): 387 397.

Brunet, Y., 1984. Modélisation des échanges sol nu atmosphère. Essai de validation locale et influence de la variabilité spatiale du sol. Thèse de l'Université Scientifique et Médicale/ Institut National Polytechnique de Grenoble.

Brutsaert, W., 1975. The roughness length for water vapor, sensible heat and other scalars. J. Atmos. Sci., 32: 2028 2031.

Camillo, P.J., Gurney, R.J. and Schmugge, T.J., 1983. A soil and atmospheric boundary layer model for evapotranspiration and soil moisture studies. Water Resour. Res., 19: 371 380.

Carslaw, H.S. and Jaeger, J.C., 1959. Conduction of heat in solids. Clarendon, Oxford, 2nd ed., 850 pp.

Cary J.W., 1979. Soil heat transducers and water vapour flow. Soil Sci. Soc. Am., J., 43: 835 839.

Constantz, J., 1982. Temperature dependence of unsaturated hydraulic conductivity of two soils. Soil Sci. Soc. Am., J., 46: 466 470.

De Vries, D.A., 1958. Simultaneous transfer of heat and moisture in porous media. Trans. Am. Geophys. Union, 39: 909 916.

De Vries, D.A., 1966. Thermal properties of soils. In: W.R. van Wijk (Editor), Physics of plant environment. North Holland, Amsterdam.

Dunand, A., 1982. Modélisation des transferts thermiques et hydriques dans le sol. Application à l'extraction d'énergie thermique par pompe à chaleur couplée à un réseau horizontal de tuyaux enterrés. Thèse de l'Université Scientifique et Médicale/Institut National Polytechnique de Grenoble.

Higuchi, M., 1984. Numerical simulation of soil water flow during drying in a non-homogeneous soil. J. Hydrol., 71: 303 334.

Idso, S.B., Jackson, R.D., Reginato, R.J., Kimball, B.A. and Nakayama, F.S., 1974. The dependence of bare soil albedo on soil water content. J. Appl. Meteorol., 14: 109 113.

Johansen, O., 1975. Thermal conductivity of soils. Ph.D. Thesis, Univ. of Trondheim, Norway.

Jury, W.A. and Letey, J., Jr., 1979. Water vapor movement in soil: reconciliation of theory and experiment. Soil Sci. Soc. Am., J., 43: 823 827.

Kay, B.D. and Groenevelt, P.H., 1974. On the interaction of water and heat in frozen and unfrozen soils. I. Basic theory: the vapor phase. Soil Sci. Soc. Am., Proc., 38: 395 400.

Lai, S.H., Tiedge, J.M. and Erickson, A.E., 1976. In situ measurement of gas diffusion coefficient in soils. Soil Sci. Soc. Am., J., 40: 3 6.

Lafolie, F. and Bruckler, L., 1988. Numerical analysis of a trickle irrigation method to measure soil crust infiltrability. Soil Sci. Soc. Am., J. (in press).

Lascano, R.J. and Van Bavel, C.H.M., 1982. Spatial variability of soil hydraulics and remotely sensed soil parameters. Soil Sci. Soc. Am., J., 46: 223 228.

Luikov, A., 1966. Heat and mass transfers in capillary porous bodies. Pergamon, Oxford.

Milly, P.C.D., 1982. Moisture and heat transport in hysteretic, inhomogeneous porous media: a matric head-based formulation and a numerical model. Water Resour. Res., 18: 489 498.

Milly, P.C.D., 1984. A simulation analysis of thermal effects on evaporation from soil. Water Resour. Res., 20: 1087 1098.

Monin, A.S. and Obukhov, A.M., 1954. Basic laws of turbulence mixing in the ground layer of the atmosphere. Tr. Geofiz. Inst. Akad. Nauk, SSSR, 24: 163 187.

Mualem, Y., 1976. A new model for predicting the hydraulic conductivity of unsaturated porous media. Water Resour. Res., 12: 513 521.

Nimmo, J.R. and Miller, E.E., 1986. The temperature dependence of isothermal moisture vs. potential characteristics of soils. Soil Sci. Soc. Am., J., 50: 1105 1113.

Passerat de Silans, A., 1986. Transferts de masse et de chaleur dans un sol stratifié soumis à une excitation atmosphérique naturelle. Comparaison modèles expérience. Thèse de Doctorat de l'Institut National Polytechnique de Grenoble.

Paulson, C.A., 1970. The mathematical representation of windspeed and temperature profiles in the unstable atmospheric surface layer. J. Appl. Meteorol., 9: 857 861.

Philip, J.R. and De Vries, D.A., 1957. Moisture movement in porous materials under temperature gradients. Trans. Am. Geophys. Union, 38: 222–232.

Priestley, C.H.B., 1959. Turbulent transfer in the lower atmosphere. Univ. of Chicago Press, Chicago, Ill.

Recan, M., 1982. Simulation numérique du comportement thermique et hydrique d'un sol nu. Application à l'étude de l'évaporation par télédétection. Thèse de Doctorat de l'Institut National Polytechnique de Toulouse.

Remson, I., Hornberger, G.M. and Moltz, J.F., 1971. Numerical methods in subsurface hydrology. Wiley, New York, N.Y., 397 pp.

Rosema, A., 1975. Simulation of the thermal behaviour of bare soils for remote sensing purposes. In: D.A. de Vries and N.H. Afgan (Editors), Heat and mass transfers in the biosphere. Wiley, New York, N.Y., pp. 109–135.

Sasamori, T., 1970. A numerical study of atmospheric and soil boundary layers. J. Atm. Sci., 27: 1123–1137.

Saugier, B., Ripley, E.A. and Lacke, P., 1974. A mechanistic model of plant growth and water use for the Matador grassland. Tech. Rep. No. 65, Univ. of Saskatchewan, Sask.

Saugier, B., 1974. Transport de CO_2 et de vapeur d'eau à l'interface végétation–atmosphère. Thèse de Doctorat ès-Sciences de l'Université des Sciences et Techniques du Languedoc, Montpellier.

Saugier, B. and Ripley, E.A., 1978. Evaluation of the aerodynamic method of determining fluxes over natural grassland. Q. J. R. Meteorol. Soc., 104: 257–270.

Schieldge, J.P., Kahle, A.B. and Alley, R.E., 1982. A numerical simulation of soil temperature and moisture variations for a bare field. Soil Sci., 133: 197–207.

Sellers, W.D., 1965. Physical Climatology. Univ. of Chicago Press, Chicago, Ill., 272 pp.

Soer, G.J.R., 1977. Model TERGRA. Niwars Publ. No. 46.

Sophocleous, M., 1979. Analysis of water and heat flow in unsaturated–saturated porous media. Water Resour. Res., 15: 1195–1206.

Thom, A.S., 1975. Momentum, mass and heat exchange of plant communities. In: J.L. Monteith (Editor), Vegetation and the Atmosphere. Academic Press, New York, N.Y., Vol 1: 57–109.

Vachaud, G., Dancette, C., Sonko, S. and Thony, J.L., 1978. Méthodes de caractérisation hydrodynamique in-situ d'un sol non saturé. Application à deux types de sol du Sénégal en vue de la détermination des termes du bilan hydrique. Ann. Agron., 29: 1–36.

Van Bavel, C.H.M. and Hillel, D.I., 1976. Calculating potential and actual evaporation from a bare soil surface by simulation of concurrent flow of water and heat. Agric. Meteorol., 17: 453–476.

Vauclin, M., Hamon, G. and Vachaud, G., 1977. Simulation of coupled flow of heat and water in partially saturated soil. In: Influence des Gradients Thermiques sur les Transferts d'Humidité dans la Zone Non Saturée. Action Thématique C.N.R.S., Paris, No. 1652.